# Competitive growth during directional solidification experiments of 〈1 1 1〉 Dendrites

# Competitive Growth during Directional Solidification Experiments of <111> Dendrites

**T. Hughes[a], A. J. Robinson[a], S. McFadden[b, a]**

[a]Department of Mechanical, Manufacturing and Biomedical Engineering, Trinity College Dublin, Ireland

[b]School of Computing, Engineering, and Intelligent Systems, Ulster University, Magee Campus, Londonderry, Northern Ireland BT487JL, United Kingdom. (permanent address)

Keywords: A1.Crystal Morphology, A1.Crystal structure, A1.Dendrites, A1.Directional solidification, A2.Growth from melt, B1.Alloys

## Abstract

Competitive growth is a key topic in directional solidification, however, to the authors' best knowledge, there are no experimental or numerical studies on competitive growth between neighbouring <111> dendrites. The secondary arms of <111> dendrites can grow with more favourable orientation than those of <100> dendrites and this has implications for the competitive growth mechanism. An experimental apparatus was developed for in-situ directional solidification with a transparent model alloy, Neopentyl Glycol-35wt.% (D)Camphor (NPG-35wt.%DC), which has <111> dendrite orientation. Seven tests were conducted with different temperature gradients and isotherm speeds to investigate competitive growth behaviour. Multiple grains were identified in each test with examples of competition at converging and diverging grain boundaries as well as obedience and disobedience with the well-known Walton-Chalmers rule. Unfavourably oriented crystal colonies at diverging grain boundaries were able to outgrow favourably oriented colonies via tertiary branching. Overgrowth by the unfavourably oriented crystal was linked to the advantageous growth directions of secondary arms in <111> dendrites. Automated dendrite tip velocity tracking further elucidated the tertiary branching mechanism that allowed the unfavourably oriented crystal colonies to stabilise along the growth direction. It is proposed that the deviation from the Walton-Chalmers rule of competitive growth is probabilistic and depends on the initial seeding as well as the 3D nature of the experiments.

# 1. Introduction

Competitive dendritic growth is a key topic in directional solidification as it influences the grain structure or crystallographic texture, and hence the material properties of as-cast parts. Preferred growth directions arise due to temperature gradients at the macro scale, where crystals with differing orientations compete to outgrow one another. Crystal arms that are well-aligned with and that are growing in the opposite direction to the heat flow have preferential orientation. The Walton-Chalmers rule [1,2], depicted in Fig. 1 [3,4], is a well-accepted description of how preferred orientations arise in directional solidification of dendrites with <100> morphology. The figure shows three neighbouring colonies of dendrites; colonies A and C with favourable orientations have their growth direction aligned with the direction of heat flux, while colony B has an unfavourable orientation and grows at some offset, $\alpha_1$, to the preferred direction. Under steady-state conditions, the liquidus isotherm advances with speed $v_L$ and well-aligned dendrites will grow at some distance behind it by matching their growth rate to the liquidus isotherm speed, $v_1 = v_L$. To maintain the required speed, the dendrite tips grow at some finite distance behind the liquidus isotherm where it can experience the required level of undercooling, $\Delta T_1$. To remain competitive, misaligned dendrites must maintain higher tip growth rates ($v_2 > v_1$) such that their vector component in the favourable direction, $v_2$', matches the isotherm speed (i.e., $v_2 = v_L/Cos(\alpha_1)$). To maintain higher growth rates, the misaligned dendrites must grow at a higher undercooling, $\Delta T_2$, which is found at a distance further behind the liquidus isotherm than the tips of the favourably oriented dendrites.

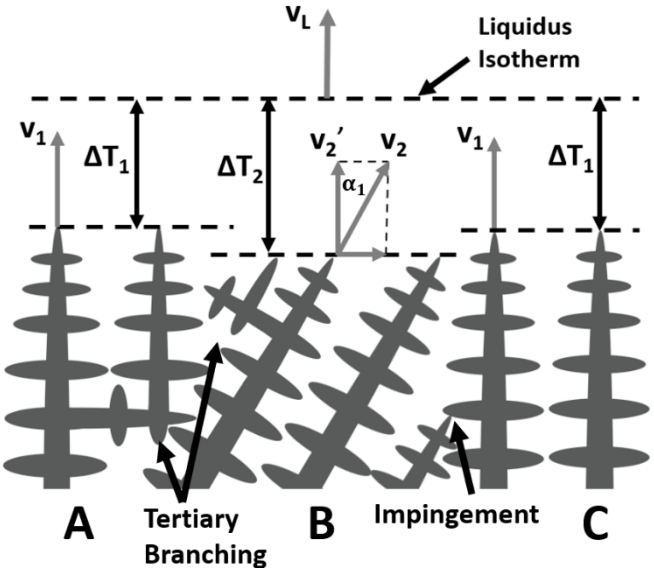


**Fig. 1** Schematic illustration of Walton-Chalmers rule adapted from [3,4]. In order to have a vertical component of velocity equal to its neighbour, the unfavourably oriented dendrite colony (B) lags the favourably oriented colonies (A and C) and grows at greater undercooling and tip velocity. Colony B impinges on colony C at the converging boundary, while colony A tends to outgrow colony B via tertiary branching at the diverging grain boundary.

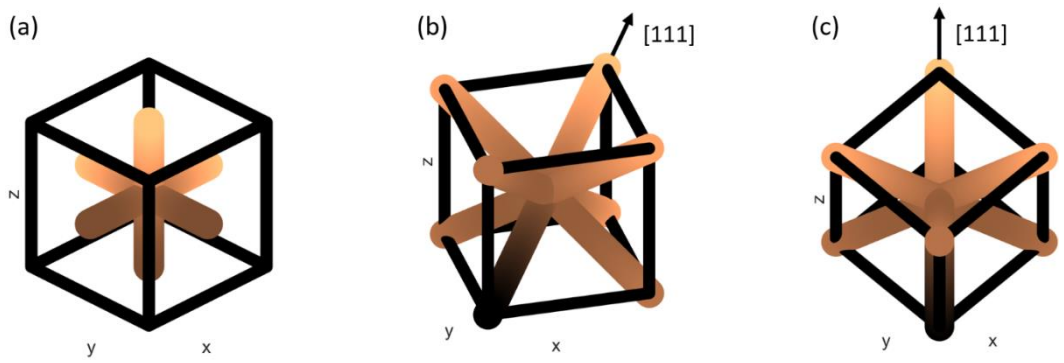


**Fig. 2** Unit cells for <100> and <111> dendrite patterns: (a) Classical <100> pattern with six growth directions (all orthogonal to each other) (b) <111> dendrite pattern with eight growth directions (c) <111> pattern viewed orthogonal to the [111] direction; a primary columnar dendrite aligned with [111] has six secondary dendrite arms; three arms subtend 70.5$^{o}$ from the primary growth axis, and the other three subtend 109.5$^{o}$.

Consequentially, neighbouring misaligned dendrites lag behind and get outgrown or blocked by their more favourably oriented counterparts. Fig. 1 shows Colony B's primary dendrite tips impinge on colony C at the grain boundary. At the AB boundary, colonies A and B compete via tertiary branching, and favourably oriented crystals A and C overgrow and eliminate the unfavourably oriented crystal, B. Thus, the Walton-Chalmers model explains the origin of preferred orientation in directional solidification, i.e., the decreased average misalignment [1] and reduced spread of the misalignment [2], which occurs due to competitive growth. The model was later validated by in-situ experiments with the SCN-ACE transparent alloy system [5].

Competitive growth is a key mechanism for columnar dendritic growth, particularly during the equiaxed-to-columnar transition and progressive columnar-to-equiaxed transition. In metal casting, a chill zone typically forms beside the mould wall in contact with the liquid melt with an initially homogenous temperature and composition. The chill zone consists of a thin layer of fine equiaxed dendrites with random orientation. Heat exits through the mould wall as the temperature gradient forms and favourably oriented arms of primary equiaxed dendrites grow directionally in opposition to the heat flux direction via the competitive mechanism described by Walton and Chalmers. After reaching a sufficient aspect ratio (typically greater than two [6]), the crystals are classified as columnar. This process is termed the Equiaxed-to-Columnar Transition (ECT). As solidification continues in the casting, temperature gradients may decrease such that the columnar dendrites lose their competitive advantage, and equiaxed solidification (with no preferential orientation) can replace the columnar structure. The process is termed the Columnar-to-Equiaxed Transition (CET). An increase in liquidus isotherm speed or a decrease in temperature gradient (or both) causes the CET. In the CET scenario, constitutional undercooling in the liquid ahead of the columnar front exceeds the heterogeneous nucleation and

free growth undercooling levels. Nucleation and growth of equiaxed crystals occur in sufficient numbers and then block the columnar front, causing the CET. Recent investigations have shown that the CET can be sharp or progressive [7-9]. In a sharp CET, equiaxed growth occurs in sufficient numbers to cause an abrupt transition from aligned columnar crystals to randomly oriented equiaxed crystals with an aspect ratio close to unity. Progressive CETs have an intermediate region where, after partial columnar blocking, the favourably oriented arms of equiaxed crystals that become embedded into the growth structure may proceed to grow competitively (as depicted in Fig. 1) and reach elongation factors greater than two [10]. Thus, competitive crystal growth is a key mechanism in both ECT and progressive CET. Several reviews of this CET are available [11,12] and studies are ongoing within this topic [13]. If the growth rate and temperature gradient can be maintained (as in the Bridgman-Stockbarger process), well-aligned columnar structures can be produced consistently.

Dendritic growth in Face Centred Cubic alloys typically occurs along <100> crystallographic directions. However, atypical growth directions are being observed in technologically important alloys, from lightweight aluminium alloys to Ni-base superalloys [14]. Examples include <110> growth in certain compositions of Al-Zn [15,16] and Al-Ge [17]. Recently, unexpected <111> growth in Al-Cu [18–21] was reported. The different growth morphologies are linked to composition-related changes in the surface-tension anisotropy distribution [15] and are likely to be influenced by the surface attachment kinetics [18]. Gudgel and Jackson [22] set up an experiment where they performed an in-situ investigation of directionally-solidified dendrites grown from an ammonium chloride-water solution (27.5wt.% $NH_4Cl$-$H_2O$). At a pulling rate (or drive velocity) of 0.04 mm/s they noticed a fluctuating growth velocity combined with an oscillating transition in the morphology; whereby, at low velocity (< 0.04 mm/s) <100> dendrites grew and at high velocity (> 0.04 mm/s) <111> growth appeared.

Since the crystals' orientation and hence the growth direction of primary dendrite tips are key in determining the competitive growth, the family of crystallographic directions along which dendrite tips can grow should undoubtedly be an important consideration. Fig. 2 shows the growth directions arising in <100> and <111> dendrites. Classical <100> dendrites can grow in six directions where secondary or higher-order dendrite arms grow orthogonally to the parent arm. With <111> patterns, dendrite arms can grow in eight directions towards each corner of a unit cell. In this case, secondary or higher-order dendrite arms can grow at either 70.53 or 109.47 degrees from the parent arm. The implications for modelling and theory of pattern formation during solidification are not yet fully understood. However, it will be argued that three secondary dendrite arm

directions of the <111> dendrites should have a 19.47-degree angular advantage compared with the secondary arms of <100> dendrites. This difference in secondary arm alignment will be shown to have consequences on the directional solidification of <111> columnar structures - this is a point that has not yet been fully characterised or realised.

Recently, a body of numerical and theoretical models of competitive growth mechanisms has been emerging for the <100> dendrite orientation [23–31]. The purpose of this study is to investigate the competitive growth mechanisms for <111> growth morphologies. An experimental setup was developed to study macrostructure structure formation during directional solidification using a binary transparent alloy Neopentyl-Glycol-35wt.%(D)-camphor (NPG-35wt.%DC) [32]. The transparent alloy in question has been shown to solidify with <100> with a composition of NPG-20wt.%DC [33] and <111> with a composition of NPG-30wt.%DC [34]. In Sturz et al. [34], a high-resolution image of an equiaxed crystal in NPG-30wt.%DC showed close agreement in terms of the dendrite morphology to an equivalent 3D phase field model of the <111> equiaxed crystal; however, the predicted growth rate from the phase field model was a factor of five too slow when compared to the experimental data. Nevertheless, the experiments in references [33] and [34] show that a dendrite orientation transitions occurs in the NPG-DC alloy system and that both <100> and <111> growth can occur. Whether the dendrite orientation transition between morphologies is solely dependent on composition or if it has a growth rate dependence (as suggested in Gudgel and Jackson [22]) is not yet fully understood. The topic requires further investigation.

In the present work, optical microscopic imaging allowed for in-situ observation and real-time visualisation of competitive columnar growth in the transparent alloy of NPG-35wt.%DC with <111> morphology. A newly developed multiple dendrite tip tracking algorithm, described in [35], augmented the in-situ footage with velocity vectors on the dendrite tips, which aided in elucidating competitive growth mechanisms. The objectives of the investigation were as follows:

- To investigate competitive crystal growth mechanisms in directionally solidified <111> crystals.
- To apply the recently-developed dendrite tip tracking algorithm to further elucidate on the mechanisms of competitive crystal growth.
- To assess the competitive crystal growth mechanisms in <111> dendritic patterns against the classic Walton-Chalmers mechanism.

Competitive crystal growth mechanisms are of particular interest to the aerospace industry for the manufacture of turbine blade and they are of fundamental interest for further modelling activity [36]. Competitive growth models have been integrated into several numerical models of directional solidification. Hence, the experimental data provided from the study proposed here will be useful for model elucidation and validation.

# 2. Methods

## 2.1 Materials

The transparent model alloy NPG-35wt.%DC was prepared from organic crystalline materials NPG and DC supplied by Sigma Aldrich (with >99% and >97% purity, respectively). The present experiments use a hypoeutectic composition of $C_0$=35wt.%, with ⟨111⟩ dendrite orientation confirmed by inspection by overlaying macrographs with a rotatable <111> reference stick model, rotated until the alignment showed agreement. The transparent model alloy was prepared in a sealed glove box under Argon atmosphere (<5ppm $H_2O$), and liquid NPG-35wt.%DC was then transferred to the experimental facility via a high-temperature gas-tight glass syringe.

## 2.2 Apparatus and Processing Conditions

Fig. 3 shows a schematic overview of the experimental facility used. The apparatus consisted of an optically transparent annular sapphire crucible with temperature controlled hot and cold zones for directional solidification. Setpoint control of temperatures, $T_H$ and $T_C$, provided controlled temperature gradient, G, cooling rate, $\dot{T}$, and hence isotherm speed, $v_L$, in the baffle zone. Automated tracking (see [35]) showed that tests reached steady state growth rates after 15 – 45 % of their total solidification length. A camera and variable lens (1.4x–13x zoom) mounted perpendicularly to the crucible's vertical axis recorded video sequences of the directional solidification in the baffle zone. For a more detailed description of the experimental apparatus and control, the reader may refer to [32].

The test material in the crucible above the cooler was brought into the liquid phase by increasing the heater's temperature to 120 $^{o}$C. To ensure a homogenous initial composition in the liquid melt before any given test, the

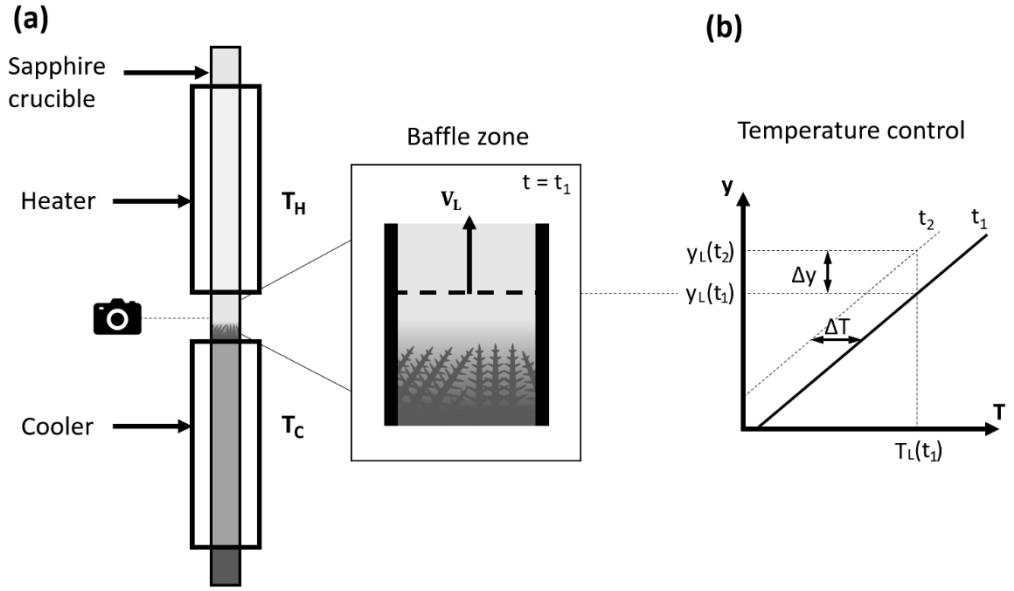


**Fig. 3** - Schematic illustration of experimental facility (a) test apparatus and magnified view of the baffle zone (b) graphical illustration of temperature control showing position of the liquidus isotherm $\mathbf{y_L}$ at time $\mathbf{t_1}$. Equal cooling rates of the heater and cooler advances the liquidus isotherm with velocity, $\mathbf{v_L}$, where $\mathbf{v_L} = (\mathbf{\Delta T/\Delta t})(\mathbf{\Delta y/\Delta T})$, or simply $\mathbf{v_L} = \dot{\mathbf{T}}/\mathbf{G}$.

**Table 1** – A list of solidification processing parameters

| Test Scenario [-] | Cooling Rate [K/min] | Temperature Gradient [K/cm] |
|---|---|---|
| 1 | 0.16 | $23.30 \pm 1.80$ |
| 2 | 0.30 | $23.58 \pm 1.83$ |
| 3 | 0.45 | $23.64 \pm 1.83$ |
| 4 | 0.16 | $16.79 \pm 1.80$ |
| 5 | 0.30 | $16.55 \pm 1.80$ |
| 6 | 0.45 | $16.57 \pm 1.41$ |
| 7 | 0.15 | $23.45 \pm 1.83$ |

baffle zone was heated with a heat gun and the heater was temporarily turned off to induce convective mixing for a period of five minutes. The heat gun was then turned off and setpoint temperatures of $T_H$ and $T_C$ were adjusted to prepare the initial temperature gradient and to position the equilibrium liquidus isotherm just inside the camera's field of view. After deactivating the heat

gun, equiaxed crystals nucleated in the liquid melt and sedimented on the top of the mushy zone providing initial seed crystals with random orientations. The initial conditions for $\mathrm{T_H}$ and $\mathrm{T_C}$ were then held for a period of at least 40 minutes and this allowed the solidification front to align with the liquidus isotherm. At that point,

ramp down cooling was initiated and optical imaging commenced. The in-situ optical footage was processed with a newly developed computer vision algorithm for automated tracking of columnar dendrite tip velocities. Additionally, a novel image-processing technique, described in the following subsection, was used to provide a detailed post-mortem image of the micro-macro structure.

## 2.3 Image Processing and Analysis

Due to the reduced opacity of the solidified structure, especially in the main bulk of the sample, microstructure detail and crystallographic features were difficult to distinguish. Microstructure detail was more discernible at the top of the mushy zone. Hence, a single, in-situ optical image of the solidifying mushy zone lacked underlying microstructure detail. To capture the columnar network development, other investigators have used manual overlay methods of images from the top of the mushy zone captured during solidification [4,37]. Here, an automatic image processing technique was developed to automate the process to show more detail of the underlying microstructure. Fig. 4 shows a schematic illustration of the image processing technique. Automatic tracking (as outlined in [32]) was used to provide the average vertical position of the top of the mushy zone, $y_f$. The image processing technique then automatically cropped a rectangular window from the given input image with the rectangle's upper left corner located at (0, $y_w$). A window height, $h_w$, was defined. The first image for any given sequence was selected based on the earliest position data provided by the tracker and subsequent images were selected corresponding to the solidification front advancing by a distance approximately equal to height of the window (within one pixel). For the first and last input images, the size of the cropped window extended to the bottom or top of the respective input image. Vertical concatenation of the cropped images then provided a single output image that facilitated assessment of the underlying microstructure. Fig. 5 shows an example of a Vertically Concatenated (VC) micrograph from test scenario 5 with manually overlaid lines to assess the misalignment of the dendrites. Dendrites arms greater than 1mm in length were deemed to have sufficient directionality to be considered in the analysis; hence secondary and tertiary arms greater than 1mm were

included in the analysis. Average and mean absolute deviation of dendrite misalignment were recorded at 30 evenly spaced vertical positions along the y-axis.

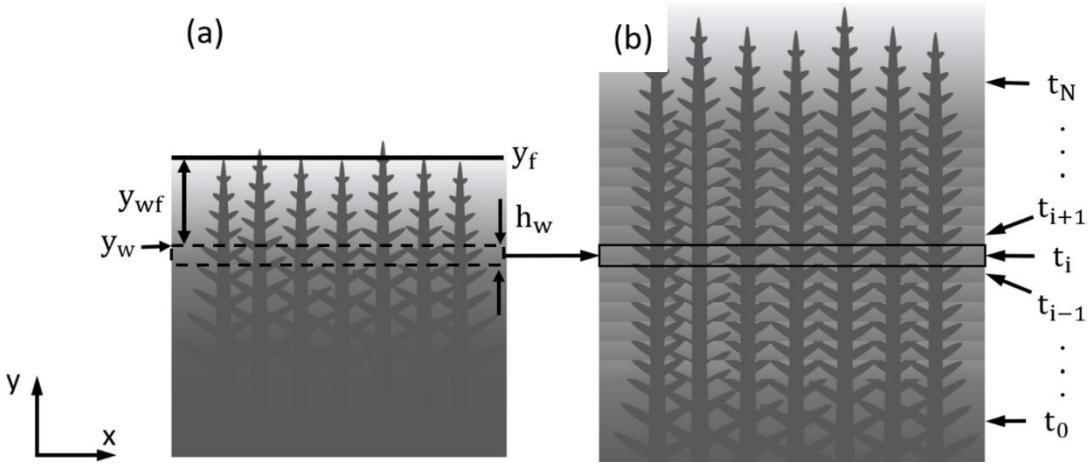


**Fig. 4** - Schematic illustration of image processing technique for developing detailed image of the microstructure (a) input image at time $\mathbf{t_i}$ with coordinates of the cropped window (b) output image from vertically concatenating windows of the selected input images.

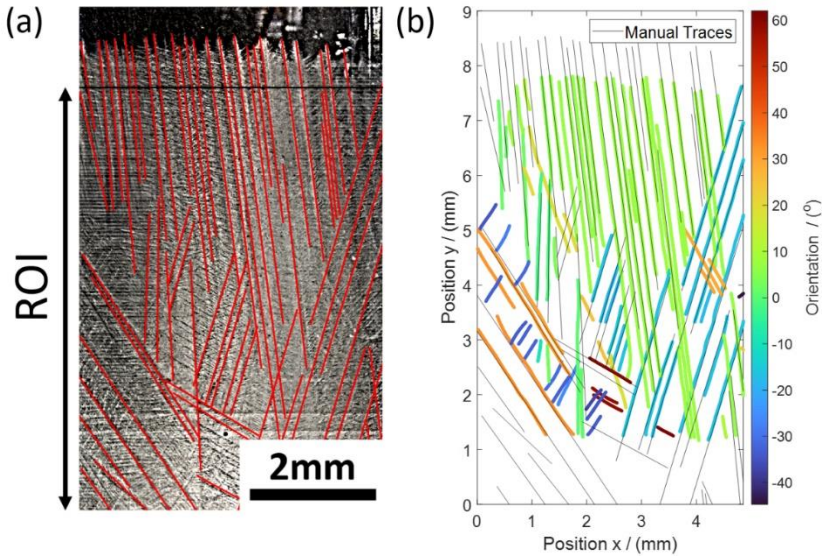


**Fig. 5** – Manual assessment of dendrite orientation showing (a) the vertically concatenated micrograph of test scenario 5 and manually overlayed dendritic skeleton (b) the automatically tracked dendrite tip positions colour mapped by orientation and comparison to manual traces shown in black.

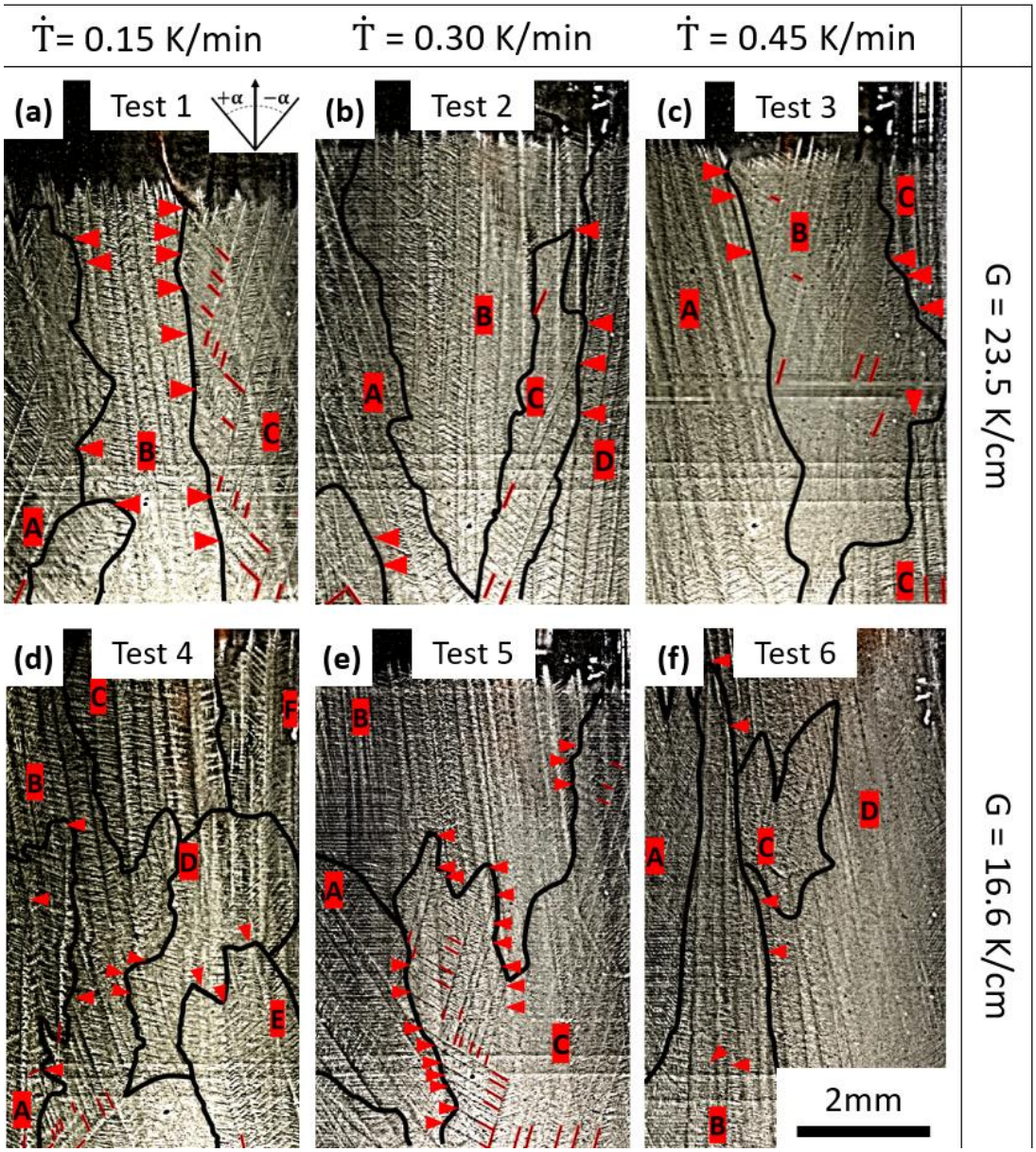


**Fig. 6** - VC micrographs showing macro-microstructure for tests 1 – 6, listed as (a) – (f), respectively. Red arrowheads show impingement, while the red/black lines highlight dendrite arm origins and the ladder structure. Grain boundaries are shown with solid black lines.

# 3. Results

As mentioned, seven directional solidification tests scenarios were conducted to investigate competitive growth in the <111> transparent alloy NPG-35wt.%DC. Fig. 6 shows the VC micrographs for test scenarios 1 to 6 with details of the thermal processing conditions on the border, while Fig. 7 shows the graphs of average dendrite misalignment, $|\bar{\alpha}|$, versus the vertical position, y. The graphs include intervals of one mean absolute deviation as a descriptive statistic of the spread of dendrite arm misalignment. Additionally, Fig. 8 (a) and (b) shows a VC

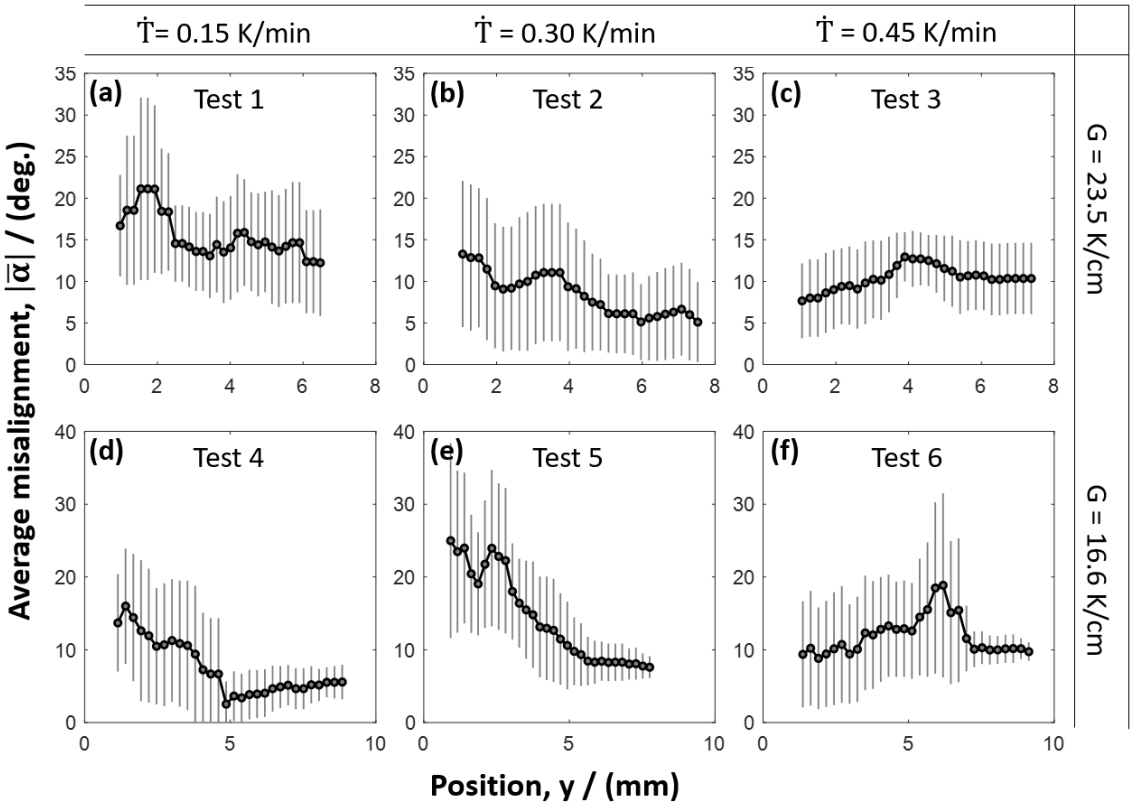


**Fig. 7** - Average misalignment $\pm$ one mean absolute deviation (as a descriptive statistic), versus y position for test scenarios 1 to 6.

micrograph and graphed results of $|\bar{\alpha}|$ versus y, corresponding to test scenario 7. In general, $|\bar{\alpha}|$ decreased with increasing, y, and is evidence that well-oriented crystals can outgrow unfavourably oriented neighbouring crystals in agreement with the Walton-Chalmers rule. In particular, test scenarios 1, 2, 4, and 5 showed obedience to the Walton-Chalmers rule with average misalignment, $|\bar{\alpha}|$, shown to decrease with increasing y. Test scenario 3 initially disobeyed then obeyed the Walton-Chalmers rule with average misalignment increasing from 7.6$^{o}$ to 13$^{o}$ but then at the 4 mm position decreasing to 10.4$^{o}$. Test 6 also showed an increase in $|\bar{\alpha}|$ but this is attributed to the presence of an embedded equiaxed grain. Contrastingly, test scenario 7 (Fig. 8) showed a steady increase in average misalignment throughout the recorded growth from 14.3 to 26.5$^{o}$. This result is evidence of disobedience with the Walton-Chalmers rule.

While the graphs of average misalignment against the vertical position, shown in Fig. 7 and Fig. 8 (b), provide a macroscopic average of competitive crystal growth, it was necessary to assess competitive crystal growth mechanisms along the individual grain boundaries. The competition occurred between multiple dendritic colonies in all seven test scenarios with examples of both diverging and converging colonies, and examples of obedience and disobedience with the Walton-Chalmers rule. A pair of crystal colonies are deemed diverging

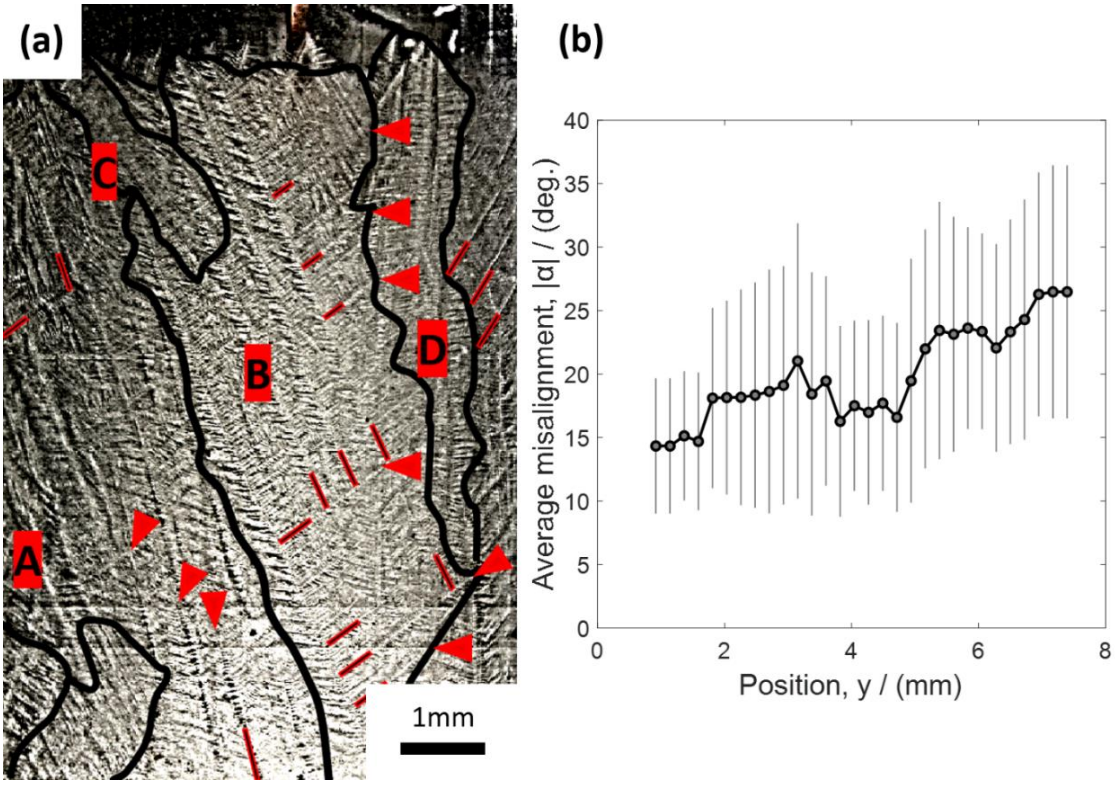


**Fig. 8** - Results of test scenario 7 processed with temperature gradient, G = 23.45 $\pm$ 1.83 K/cm, and cooling rate $\dot{\mathbf{T}}$ = 0.15 K/min (a) vertical concatenation image showing underlying micro – macro structure (b) average dendrite misalignment versus position.

when the crystals' primary growth directions point away from each other in the image plane whereas two crystal colonies are deemed converging when the primary growth directions point towards each other in image plane. Fig. 6 and Fig. 8 (a) show the colonies and grain boundaries identified in each test scenario (annotated A, B, C, etc.). Black contours indicate the grain boundaries between colonies of directionally aligned dendrites and red arrowheads highlight dendrite impingement points. The list of dendritic colonies for each test scenario, their primary growth direction, $\alpha_1$ and competitive secondary directions, $\alpha_2$, are listed in Table 2. Orientations $\alpha_1$ and $\alpha_2$ are provided with respect to the vertical axis (see reference axis and convention in Fig. 6 (a)). Table 2 also lists the grain boundaries; the relative orientation of the neighbouring crystals (i.e., whether they were converging or diverging from one another); and whether they displayed obedience or disobedience to the Walton-Chalmers rule. Grain boundaries with orientations greater than 45$^o$ were omitted because the competition was assumed to occur predominantly due to misalignment about the x-axis. Descriptions of the outcomes from each test scenario are provided in the following paragraphs.

Test scenario 1, shown in Fig. 6 (a) and Fig. 7 (a), showed a small decrease in average misalignment, $|\bar{\alpha}|$, from 16.7$^o$ to 12.2$^o$. Two grain-boundaries formed in this test with converging growth at the AB boundary and

diverging growth at the BC boundary. Competition at grain boundary AB obeyed the Walton-Chalmers rule where the favourably oriented colony, B, tended to outgrow colony A. However, competition at boundary BC disobeyed the Walton-Chalmers rule since the less favourably oriented colony C tended to outgrow colony B by forming a ladder of tertiary branches at the grain boundary. The success of C at the diverging boundary was due to the orientation compared with B, $\alpha_{1,C} = -16^{o}$ and $\alpha_{1,B} = 7^{o}$, which allowed secondary arms of C to be more favourably oriented and better able to compete with the secondary arms of crystal colony B. The favourably oriented crystal colony B was consistently overgrown by this mechanism.

Fig. 6 (b) shows test scenario 2. Most grain boundaries that formed in this scenario obeyed the Walton-Chalmers rule. For example, colony B, with $\alpha_{1,B} = 0^{o}$, tended to overgrow unfavourably oriented colonies A ($\alpha_{1,A} = 18^{o}$) and C ($\alpha_{1,C} = -22^{o}$). Colony C, was less favourably oriented compared with neighbouring colonies B and D ($\alpha_{1,D} = -8^{o}$); at the diverging boundary between B and C, colony C was overgrown by B. At the converging CD boundary, colony C tended to overgrow the favourably oriented colony D. A higher overgrowth rate by B on C compared with C on D ultimately led to C's elimination. The CD boundary was the only case in test scenario 2 that showed disobedience with the Walton-Chalmers rule. Fig. 7 (b) shows that test scenario 2 generally obeyed the Walton-Chalmers rule, where misalignment decreased throughout and, in general, the mean absolute deviation also reduced.

Test scenario 3, shown in Fig. 6 (c) and Fig. 7 (c), shows colony C ($\alpha_{1,C} = 3^{o}$) with favourable orientation initially overgrown by its neighbour B ($\alpha_{1,B} = -15^{o}$) causing the average misalignment to increase, but then C begins to overgrow B again. Colony B, diverging from colony A ($\alpha_{1,A} = 13^{o}$), also tended to outgrow colony A with periodic tertiary branching.

Test scenario 4 showed a decreasing $|\bar{\alpha}|$ and a decreasing mean absolute deviation. In general, the trends obeyed the Walton-Chalmers rule, with unfavourably oriented colonies B and E being overgrown. However, colony A with $\alpha_{1,A} = 0^{o}$, was overgrown by colony B.

Test scenario 5, shown in Fig. 6 and Fig. 7 (e), shows obedience to the Walton-Chalmers rule with decreased average misalignment and mean absolute deviation showing convergence to a single preferential orientation. A single colony of dendrites, B, with a misalignment of $\alpha_{1,B} = 7^{o}$ tended to overgrow colonies A and C ($\alpha_{1,A} = 33^{o}$ and $\alpha_{1,C} = -17^{o}$). Correspondingly, the graph in Fig. 6 (e) shows an average misorientation converging on $7^{o}$.

In test scenario 6 (Fig. 6 and Fig. 7 (f)), colony D tended to outgrow its neighbours B and A. An equiaxed crystal (C) nucleated ahead of the columnar front and blocked growth in this area as it settled into and became embedded into the columnar structure. The more favourably oriented arms of the equiaxed crystal ($\alpha_{1,C} = -19^{o}$) continued to grow and competed with colonies B ($\alpha_{1,B} = -1^{o}$) and D ($\alpha_{1,D} = 10^{o}$) but were shortly

**Table 2** - Summary of crystal misalignment (primary growth direction, $\boldsymbol{\alpha_1}$ and competitive secondary directions, $\boldsymbol{\alpha_2}$) and observations of obedience or disobedience with the Walton-Chalmers rule at each grain boundary.

| | | | Grain Boundary and Comments | |
|---|---|---|---|---|
| | $\alpha_1$ | $\alpha_2$ | Boundary | Comments |
| Units | degree | degree | | |
| Test Scenario 1 | | | | |
| Colony A | -20 | 40 | AB | converging obeys |
| Colony B | 7 | | BC | diverging disobeys |
| Colony C | -16 | 44 | | |
| Test Scenario 2 | | | | |
| Colony A | 18 | | AB | diverging obeys |
| Colony B | 0 | | BC | diverging obeys |
| Colony C | -22 | | BD | diverging obeys |
| Colony D | -8 | | CD | converging disobeys |
| Test Scenario 3 | | | | |
| Colony A | 13 | | AB | diverging disobeys |
| Colony B | -15 | | BC | converging disobeys then obeys |
| Colony C | 3 | | | |
| Test Scenario 4 | | | | |
| Colony A | 0 | | AB | converging disobeys |
| Colony B | 10 | | BC | diverging obeys |
| Colony C | 4 | | | |
| Colony D | 1 | | | |
| Colony E | 17 | | | |
| Colony F | -2 | | | |
| Test Scenario 5 | | | | |
| Colony A | 33 | | AB | diverging obeys |
| Colony B | 7 | | BC | converging/diverging obeys |
| Colony C | -17 | 58 | CD | converging obeys |
| Colony D | 24 | | | |
| Test Scenario 6 | | | | |
| Colony A | -19 | | AB | converging disobeys |
| Colony B | -1 | | BD | converging disobeys |
| Colony C | -19 | | | |
| Colony D | 10 | | | |
| Test Scenario 7 | | | | |
| Colony A | 17 | | AB | converging disobeys |
| Colony B | 24 | -53 | BD | diverging obeys |
| Colony C | 40 | | | |
| Colony D | -3 | | | |
| Colony E | 1 | -30 | | |

outgrown by the more favourably oriented colony B. Correspondingly, Fig. 7 (f) shows the increase in average dendrite misalignment between 5mm and 7mm in the vicinity of the elongated equiaxed grain.

In contrast to the trends observed in tests 1 to 6, test scenario 7, under similar processing conditions as test 1, showed that dendrite alignment did not follow the Walton-Chalmers rule. Fig. 8 (a) shows the average dendrite misalignment, which tended to increase throughout the experiment. The increase was partly due to the competitive secondary arms of colony B where $\alpha_{1,B} = 24^{o}$ and $\alpha_{2,B} = -53^{o}$, and colony E where $\alpha_{1,E} = 1^{o}$ and $\alpha_{2,E} = -30^{o}$, but also colony C which emerged further up with $\alpha_{1,C} = -40^{o}$. At the diverging BD boundary where $\alpha_{1,B} = 24^{o}$ and $\alpha_{1,D} = -3^{o}$, colony D tended to overgrow colony B, but B was largely stabilised due to competitive secondary arms. Consequentially, the average misalignment increased from $14^{o}$ to $27^{o}$.

Fig. 9 shows a close-up image sequence from test 5 in the upper right area of colony D (see Fig. 6 (f)) with a primary growth direction of $\alpha_{1,D} = -19^{o}$ and primary dendrite tip velocities that ranged from 4.5 to 5 µm/s. The secondary arms with $\alpha_{2,D} = 48^{o}$ grew at approximately 7 µm/s. Supplementary video data is available on the journal website. The observed trends between the growth vectors and the resulting final grain textures are discussed in greater detail in the next section.

Fig. 10 shows the development of the grain boundary in test 5 between diverging colonies A and C. Colony C periodically formed tertiary branches and ladder structures with alternating success between arms growing along with the primary [111] and secondary $[1\bar{1}1]$ directions. Video evidence (provided as supplementary data on the journal's website) shows that an opening formed between the diverging colonies A and C, and secondary arms grew into the open region. Fig. 10 (d)-(e), show a tertiary arm extending along the crystals [111] direction was able to break out and block the newer secondary dendrite arms, which were further up the primary trunk. As solidification proceeded, the [111] tertiary arms eventually became primary arms themselves. The secondary arms of the initial primary dendrite did not compete any further as their pathways were blocked by its neighbour's successful tertiary arms.

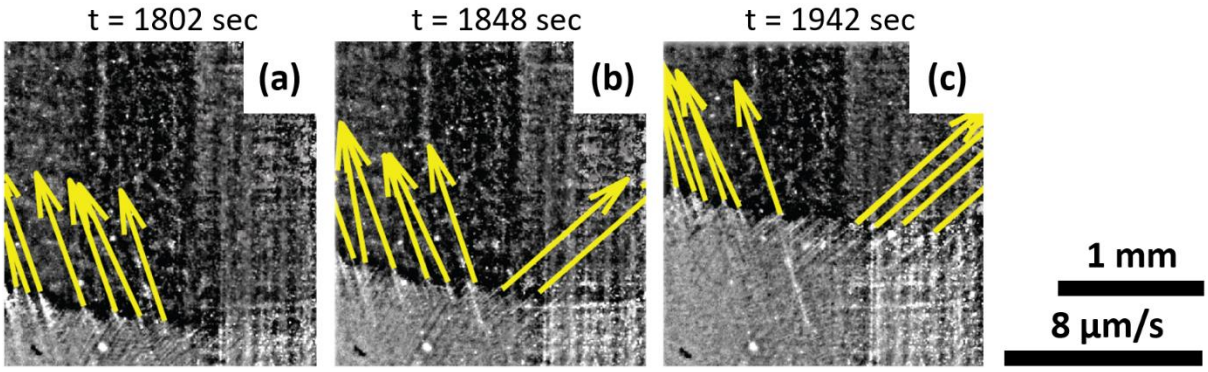


**Fig. 9** - Optical image sequence showing dendrite tip tracking on crystal D, test 6. The image sequence shows a colony of secondary dendrite arms from crystal D growing with higher misalignment and tip velocity.

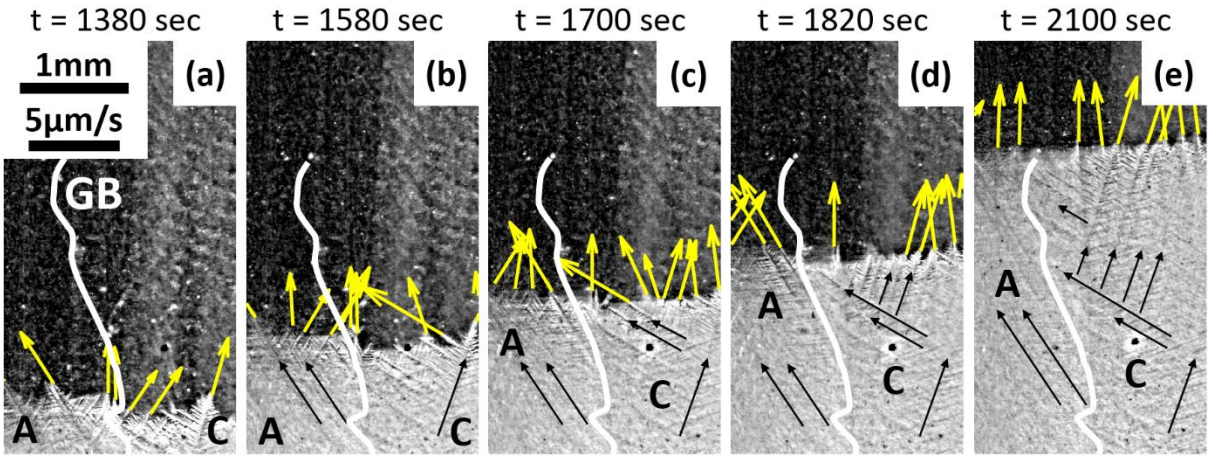


**Fig. 10** - Optical image sequence from test 5 with dendrite tip tracking showing grain boundary formation for diverging crystals colonies A and C. Colony C's secondary arms grow into and fill the space between the diverging grains and repeated tertiary branching forms a ladder structure in colony C.

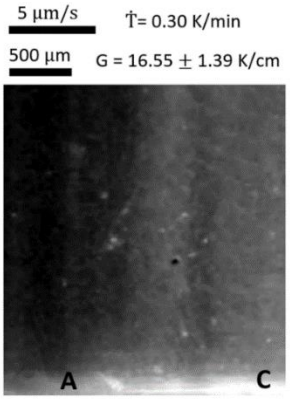


**Vid. 1.** Augmented video data showing close-up view of competitive growth in Test 5. With competitive secondary dendrite arms of grain C overgrowing grain A.

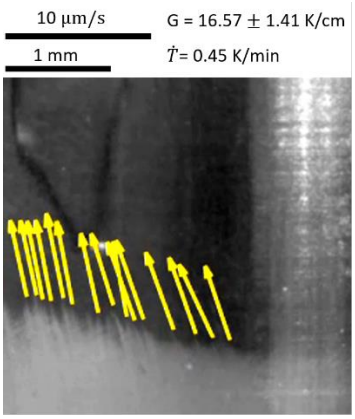


**Vid. 2**. Augmented video data showing a close-up view of competitive secondary dendrite arms from Test 6. (Note to reviewers: these are placeholders for the videos, please see the supplementary video data attached further down in this document).

# 4. Discussion

Competitive directional crystal growth mechanisms emanating from randomly oriented seed crystals have been investigated with seven directional solidification tests. Multiple colonies formed in each test scenario with examples of both diverging and converging boundaries, as well as obedience and disobedience with the Walton-Chalmers rule. The analyses were aided by a newly developed computer vision algorithm that provided automatic tracking of the positions and velocity vectors for multiple columnar dendrite tips observed within each experiment. The results indicate that scenarios that disobeyed the classical Walton-Chalmers rule, that is, by the unfavourably oriented crystals tending to overgrow the favourably oriented crystals, occurred due to preferential tertiary branching from the unfavourably oriented crystal colonies (the mechanism is depicted in Fig. 11 (b)).

Tertiary branching occurs in single-crystal directional solidification when the primary growth direction is not aligned with the direction of heat flow [37,38] or when columnar crystals pass a re-entrant corner in a mould [4]. Gandin et al. [40] examined tertiary branching as a competition mechanism for a divergent bicrystal using the <100> succinonitrile-acetone system. They demonstrated that with higher misalignment, the unfavourably oriented crystal could compete with a favourably oriented crystal via tertiary branching. However, with reduced misalignment, the unfavourably oriented crystal's secondary arms became suppressed, preventing tertiary branching in the unfavourably oriented crystal and instead allowed successful tertiary branching in the

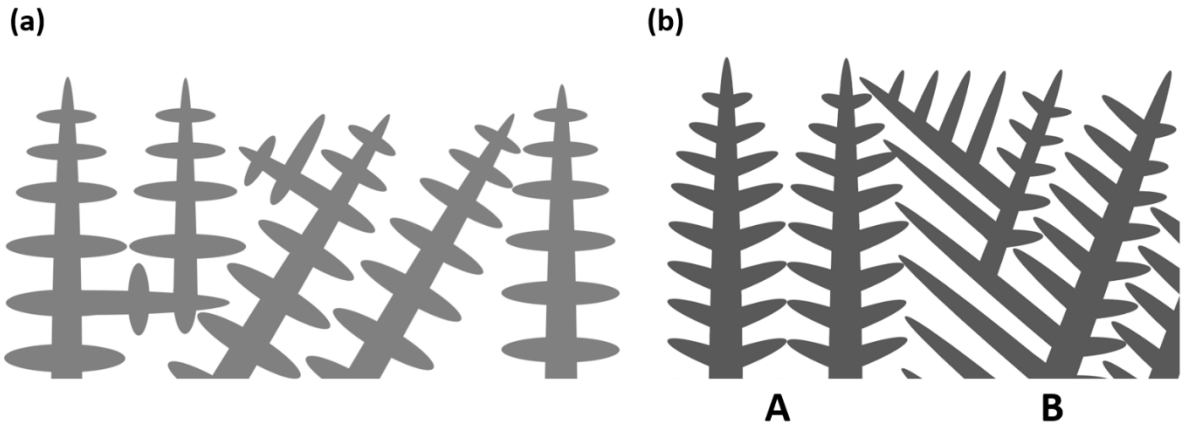


**Fig. 11** – (a) Schematic illustration of the Walton-Chalmers model with <100> dendrites. (b) Schematic illustration of divergent boundary with <111> dendrites. The schematic shows competition between favourably oriented colony, A, and unfavourably oriented colony, B, with $\boldsymbol{\alpha_{1,A} = 0^o}$ and $\boldsymbol{\alpha_{1,B} = -20^o}$. Competitive secondary arms and branching by colony B allow it to maintain a grain boundary parallel to the primary growth direction of A.

favourably oriented crystal. Wagner et al. also showed the unfavourably oriented crystal stabilising against the favourably oriented crystal by the same mechanism [41]. In all of these examples with <100> dendrites, the unfavourably oriented crystals were misaligned by more than 33$^o$. This manuscript highlights multiple instances where the misaligned crystals competed by periodic tertiary branching (see colony C in test scenario 1, colony B in test scenario 3, colony C in test scenario 5, and colony B in test scenario 7). However, in contrast to other examples [40,41], tertiary branching was favoured in the unfavourably oriented crystals with a misalignment as low as 16$^o$ (colony C, test 1). It is likely that this behaviour is a consequence of the <111> structure where secondary arms have a 19.5$^o$ advantage compared with the <100> configuration.

The average misalignment results (Fig. 7 and Fig. 8 (b)) provided a macroscopic average of the competitive crystal growth, where decreasing average and reduction in the variance of the measured misalignment indicates an average agreement with the Walton-Chalmers rule [1,2]. In this study, the majority of scenarios ultimately tended to agree with the Walton-Chalmers rule by showing either a decrease in the average misalignment or convergence to a single preferential orientation. However, in test scenario 7, the results were significantly different with the average misalignment increasing over the solidification length instead of decreasing and with approximately uniform variance. Moreover, thermal processing conditions of cooling rate and temperature gradient applied in test scenario 7 were the same as test scenario 1. Thus, with similar parameters applied, the different outcomes that were observed were stochastic in nature. The results showed that some pairs of crystal orientations allow the unfavourably oriented crystal to overgrow its favourably oriented neighbour. Hence,

depending on the initial seeding, the average misalignment could also increase. The stochastic nature of the outcome is likely dependent on the initial seeding orientations.

It is important to note that the Walton-Chalmers rule, depicted in Fig. 1, is a 2D description of competitive growth during directional solidification. However, the experiments' 3D nature and crystal colonies' 3D orientation likely affected competitive growth mechanisms and contributed to the observed deviations from the Walton-Chalmers rule. For example, secondary arms of adjacent crystal colonies do not necessarily align or compete in direct opposition; the crystals can have some finite rotation about their primary growth direction, altering the competition mechanism (see Fig. 12 in [23]). The crystals' misalignment about the x-axis could also affect the mechanisms of competitive growth. Fig. 6 and Fig. 8 (a) show some crystal colonies which emerged from behind other crystal colonies, for example, colony C in test 4 and colony B in test 5, and is evidence of the experiments 3D nature. Assuming obedience to the Walton-Chalmers rule, the crystal colonies overgrown by colony C in test 4 and colony B in test 5 had a sufficient rotation about the x-axis towards the crucible wall to impinge on it and be overgrown. The crucible's cylindrical geometry also means that, depending on the crystal's misalignment about the x-axis, crystal colonies with components in the positive or negative x-direction have a greater chance of impinging the crucible wall. On the other hand, several crystals showed evidence of low misalignment about the x-axis as well as the image plane, where one or more of the crystal colonies' dendrite arms could persist at the front of the crucible for the majority of the experiment (for example, test 1, colony B; test 2 colonies B and D; test 3 colonies A and C; test 6 colonies B and D). For more significant misalignments about the x-axis, the most extended dendrite arm of those colonies would have been impeded by the crucible wall and outgrown or migrated towards the crucible's centreline axis and out of the camera's view. Some boundaries could also have been affected by a third crystal colony competing in the background (i.e. out of sight in Fig. 6 and Fig. 8 (a)) in which case the Walton-Chalmers rule does not fully describe the competition, for example towards the end of the CD boundary in test 2 it is clear that colonies B, C and D compete close to the front of the crucible. However, the area where three crystal colonies compete simultaneously is relatively much less than areas where just two crystals compete. Thus, it is fair to assume that most of the boundaries in Fig. 6 and Fig. 8 (a) comprise two crystal colonies in competition.

Further experiments capable of assessing the 3D crystal orientation are required to fully understand the mechanisms of competition and specifically the outcome in test scenario 7. To confirm the growth as <111>, the

present work proceeded by inspecting the growth directions on the micrographs and comparing them to simplified <111> 3D stick models of the dendrite morphology. This approach was also used by Sturz et al. [42] where the stick model was rotated to match the growth directions projected by each crystal colony, which confirmed to some extent the <111> nature of the morphology.

# 5. Conclusions

Seven separate scenarios of directional solidification were conducted with controlled cooling rate and temperature gradient; and hence, isotherm speed to investigate competitive growth mechanisms in <111> crystals. In-situ footage of the columnar growth was augmented with a bespoke dendrite tip tracking algorithm to provide velocity vectors at the dendrite tips; this provided an improved qualitative insight into the mechanisms of competitive growth. This work has provided the first examples of competitive crystal growth with associated tip velocity vectors in directionally solidified <111> crystals.

Specific experimental results generally followed the Walton-Chalmers predicted growth behaviour, that is, a decrease in average misalignment due to favourably oriented crystals outgrowing unfavourably oriented crystal. However, there were instances when the Walton-Chalmers rule was disobeyed since no convergence to a single preferred orientation was demonstrated. In contradiction to the Walton-Chalmers rule, the average misalignment of test scenario 7 increased from $14^{o}$ to $28^{o}$ over the length of the observed solidification. Moreover, test scenario 1, under the same conditions as test scenario 7 obeyed the Walton-Chalmers rule. It is proposed that the deviation from the Walton-Chalmers rule of competitive growth is probabilistic and likely depends on the initial seeding as well as the 3D nature of the experiments.

Competition mechanisms at 17 grain-boundaries were detailed in Table 2 with multiple examples of diverging and converging boundaries provided. Obedience and disobedience to the Walton-Chalmers rule was highlighted with no clear trend to predict whether the rule should be obeyed or not. However, a common observation in all experiments was the ability of secondary and tertiary dendrite arms to compete with the primary arms of neighbouring colonies. In particular, the unfavourably oriented crystals were able to maintain their boundaries with the favourably oriented crystals under divergent neighbouring growth scenarios. Moreover, when the favourably oriented crystals had some misalignment, the unfavourably oriented crystals could overgrow the favourably oriented crystals parallel to the primary growth direction of the favourably oriented crystals, for example, boundary BC in test scenario 1. A similar mechanism has already been shown in <100> crystals [40,41]; however, in those scenarios, the unfavourably oriented crystals had at least $33^{o}$ misalignment, which allowed secondary arms of those <100> dendrites to achieve sufficiently favourable growth direction and dominate secondary arms of other favourably oriented crystals. In contrast, this manuscript's results showed the same mechanism occurring but with the unfavourably oriented crystals oriented at $16^{o}$. The difference is due to the

favourable crystallographic growth direction of secondary arms in <111> dendrites, i.e., the 19.5$^{o}$ advantage compared with the <100> dendrites. Hence, directional solidification with <111> crystallographic orientations has a higher probability of disobeying the Walton-Chalmers rule than <100> crystals.

It is noted that the Walton-Chalmers rule was initially intended and based on experiments with <100> dendritic growth. While several scenarios showed obedience to the Walton-Chalmers rule, this work contributes to the increasing number of experimentally observed scenarios [28,29,41,43,44] that, in addition to the Walton-Chalmers rule, should be addressed in numerical and theoretical models. The results are novel and provide the first exploration of competitive growth in <111> dendrites, however, further experiments are required to study the selection mechanism in depth and to study the 3D nature of the experiments in more detail. Additionally, further work that compares competitive growth in <100> and <111> dendrites will provide a useful benchmark for validating numerical and theoretical models of competitive growth.

## Acknowledgements

This work was supported by the European Space Agency (ESA) [contract number 4200014313NL/SH, CCN009 to AO-99-117] and by ESA PRODEX [contract number 4000110385 CN 3] as part of the CETSOL Microgravity Application Programme. ESA PRODEX funding is managed by the Irish Space Delegation at Enterprise Ireland.

## Data availability

The raw/processed data required to reproduce these findings cannot be shared at this time due to technical or time limitations.

## References

[1] D. Walton, B. Chalmers, The Origin of the Preferred Orientation in the Columnar Zone of Ingots, Trans. Metall. Soc. AIME, Vol. 215. 215 (1959) 3–13.

[2] B. Chalmers, Principles of solidification, New York, N.Y., Wiley, 1964.

[3] M. Rappaz, C.A. Gandin, Probabilistic modelling of microstructure formation in solidification processes, Acta Metall. Mater. 41 (1993) 345–360. https://doi.org/10.1016/0956-7151(93)90065-Z.

[4] M. Rappaz, C.-A. Gandin, J.-L. Desbiolles, P. Thevoz, Prediction of grain structure in various solidification processes, Metall. Mater. Trans. A. 27A (1996) 695–705. https://www.esi-group.com/sites/default/files/resource/publication/1672/s_mi.cafepredictionofgrainmmt96.pdf (accessed August 10, 2017).

[5] H. Esaka, H. Daimon, Y. Natsume, K. Ohsasa, M. Tamura, Growth Direction of Cellular and Dendritic Interface in a Constrained Growth Condition, Mater. Trans. 43 (2002) 1312–1317. https://doi.org/10.2320/matertrans.43.1312.

[6] J.D. Hunt, Steady state columnar and equiaxed growth of dendrites and eutectic, Mater. Sci. Eng. 65 (1984) 75–83. https://doi.org/10.1016/0025-5416(84)90201-5.

[7] D.R. Liu, N. Mangelinck-Noël, C.A. Gandin, G. Zimmermann, L. Sturz, H. Nguyen Thi, B. Billia, Structures in directionally solidified Al-7 wt.% Si alloys: Benchmark experiments under microgravity, Acta Mater. 64 (2014) 253–265. https://doi.org/10.1016/j.actamat.2013.10.038.

[8] Y.Z. Li, N. Mangelinck-Noël, G. Zimmermann, L. Sturz, H. Nguyen-Thi, Effect of solidification conditions and surface pores on the microstructure and columnar-to-equiaxed transition in solidification under microgravity, J. Alloys Compd. 749 (2018) 344–354. https://doi.org/10.1016/j.jallcom.2018.03.300.

[9] R.P. Mooney, L. Sturz, G. Zimmermann, N. Mangelinck-no, H. Nguyen-thi, Y. Li, D.J. Browne, S. McFadden, Concurrent model for sharp and progressive columnar to equiaxed transitions validated by directional solidification experiments processed in microgravity conditions, Comput. Mater. Sci. 210 (2022) 111436. https://doi.org/10.1016/j.commatsci.2022.111436

[10] L. Sturz, M. Wu, G. Zimmermann, A. Ludwig, M. Ahmadein, Benchmark experiments and numerical modelling of the columnar-equiaxed dendritic growth in the transparent alloy Neopentylglycol-(d)Camphor, IOP Conf. Ser. Mater. Sci. Eng. 84 (2015) 012086. https://doi.org/10.1088/1757-899X/84/1/012086.

[11] J.A. Spittle, Columnar to equiaxed grain transition in as solidified alloys, Int. Mater. Rev. 51 (2006) 247–269. https://doi.org/10.1179/174328006X102493.

[12] W.U. Mirihanage, H. Dai, H. Dong, D.J. Browne, Computational modeling of columnar to equiaxed

transition in alloy solidification, Adv. Eng. Mater. 15 (2013) 216–229. https://doi.org/10.1002/adem.201200220.

[13] G. Zimmermann, L. Sturz, H. Nguyen-Thi, N. Mangelinck-Noel, Y.Z. Li, C.A. Gandin, R. Fleurisson, G. Guillemot, S. McFadden, R.P. Mooney, P. Voorhees, A. Roosz, A. Ronaföldi, C. Beckermann, A. Karma, C.H. Chen, N. Warnken, A. Saad, G.U. Grün, M. Grohn, I. Poitrault, T. Pehl, I. Nagy, D. Todt, O. Minster, W. Sillekens, Columnar and Equiaxed Solidification of Al-7 wt.% Si Alloys in Reduced Gravity in the Framework of the CETSOL Project, JOM. 69 (2017) 1269–1279. https://doi.org/10.1007/s11837-017-2397-4.

[14] Y. Mori, H. Harada, T. Yokokawa, T. Kobayashi, S. Suzuki, Directionally-solidified dendrite morphology with eight secondary arms in an FCC ordered phase alloy, J. Cryst. Growth. 500 (2018) 15–22. https://doi.org/10.1016/j.jcrysgro.2018.07.036.

[15] T. Haxhimali, A. Karma, F. Gonzales, M. Rappaz, Orientation selection in dendritic evolution, Nat. Mater. 5 (2006) 660–664. https://doi.org/10.1038/nmat1693.

[16] F. Gonzales, M. Rappaz, Dendrite growth directions in aluminum-zinc alloys, Metall. Mater. Trans. A Phys. Metall. Mater. Sci. 37 (2006) 2797–2806. https://doi.org/10.1007/BF02586112.

[17] M. Becker, J.A. Dantzig, M. Kolbe, S.T. Wiese, F. Kargl, Dendrite orientation transition in Al–Ge alloys, Acta Mater. 165 (2019) 666–677. https://doi.org/10.1016/j.actamat.2018.12.001.

[18] M. Bedel, G. Reinhart, C.A. Gandin, A.A. Bogno, H. Nguyen-Thi, H. Henein, Evolution of the dendritic morphology with the solidification velocity in rapidly solidified Al-4.5wt.%Cu droplets, IOP Conf. Ser. Mater. Sci. Eng. 84 (2015). https://doi.org/10.1088/1757-899X/84/1/012016.

[19] M. Bedel, G. Reinhart, A.-A. Bogno, C.-A. Gandin, S. Jacomet, E. Boller, H. Nguyen-Thi, H. Henein, Characterization of dendrite morphologies in rapidly solidified Al–4.5wt.%Cu droplets, Acta Mater. 89 (2015) 234–246. https://doi.org/https://doi.org/10.1016/j.actamat.2015.02.007.

[20] M. Bedel, G. Reinhart, A.A. Bogno, H. Nguyen-Thi, E. Boller, C.A. Gandin, H. Henein, Dendrite growth morphologies in rapidly solidified Al-4.5wt.%Cu droplets, IOP Conf. Ser. Mater. Sci. Eng. 117 (2016). https://doi.org/10.1088/1757-899X/117/1/012055.

[21] H. Henein, A.A. Bogno, W. Hearn, J. Valloton, Metastable Dendrite Morphologies in Aluminum Alloys, J. Phase Equilibria Diffus. 41 (2020) 784–792. https://doi.org/10.1007/s11669-020-00833-1.

[22] K.A. Gudgel, K.A. Jackson, Oscillatory growth of directionally solidified ammonium chloride dendrites, J. Cryst. Growth. 225 (2001) 264–267. https://doi.org/10.1016/S0022-0248(01)00847-8.

[23] D. Tourret, A. Karma, Growth competition of columnar dendritic grains: A phase-field study, Acta Mater. 82 (2015) 64–83. https://doi.org/10.1016/j.actamat.2014.08.049.

[24] D. Tourret, Y. Song, A.J. Clarke, A. Karma, Grain growth competition during thin-sample directional solidification of dendritic microstructures: A phase-field study, Acta Mater. 122 (2017) 220–235. https://doi.org/10.1016/j.actamat.2016.09.055.

[25] T. Takaki, S. Sakane, M. Ohno, Y. Shibuta, T. Aoki, C.A. Gandin, Competitive grain growth during directional solidification of a polycrystalline binary alloy: Three-dimensional large-scale phase-field study, Materialia. 1 (2018) 104–113. https://doi.org/10.1016/j.mtla.2018.05.002.

[26] T. Takaki, S. Sakane, M. Ohno, Y. Shibuta, Competitive growth during directional solidification of a binary alloy with natural convection: Two–dimensional phase–field study, Model. Simul. Mater. Sci. Eng. (2019). https://doi.org/10.1088/1361- 651X/ab1a17.

[27] J. Lee, M. Ohno, Y. Shibuta, T. Takaki, Uniquely selected primary dendrite arm spacing during competitive growth of columnar grains in Al–Cu alloy, J. Cryst. Growth. 558 (2021) 126014. https://doi.org/10.1016/j.jcrysgro.2020.126014.

[28] Y.Z. Zhou, A. Volek, N.R. Green, Mechanism of competitive grain growth in directional solidification of a nickel-base superalloy, Acta Mater. 56 (2008) 2631–2637. https://doi.org/10.1016/j.actamat.2008.02.022.

[29] X.B. Meng, Q. Lu, X.L. Zhang, J.G. Li, Z.Q. Chen, Y.H. Wang, Y.Z. Zhou, T. Jin, X.F. Sun, Z.Q. Hu, Mechanism of competitive growth during directional solidification of a nickel-base superalloy in a three-dimensional reference frame, Acta Mater. 60 (2012) 3965–3975. https://doi.org/10.1016/j.actamat.2012.04.002.

[30] A. Pineau, G. Guillemot, D. Tourret, A. Karma, C.A. Gandin, Growth competition between columnar dendritic grains – Cellular automaton versus phase field modeling, Acta Mater. 155 (2018) 286–301.

https://doi.org/10.1016/j.actamat.2018.05.032.

[31] E. Dorari, K. Ji, G. Guillemot, C.-A. Gandin, A. Karma, Growth competition between columnar dendritic grains – The role of microstructural length scales, Acta Mater. 223 (2022) 117395. https://doi.org/https://doi.org/10.1016/j.actamat.2021.117395.

[32] T. Hughes, S. McFadden, A.J. Robinson, A front-tracking measurement technique for in-situ columnar and equiaxed structure growth with controlled solidification, Meas. Sci. Technol. 32 (2020) 045903. https://doi.org/10.1088/1361-6501/abcb24.

[33] G. Zimmermann, M. Hamacher, L. Sturz, In-situ observation of equiaxed dendrites solidifying under reduced gravity conditions during the TEXUS-55 mission – The MEDI-2 experiment, Proc. 24rd ESA Symp. Eur. Rocket Balloon Program. Relat. Res. (2019)

[34] L. Sturz, M. Hamacher, J. Eiken, G. Zimmermann, V. Access, E.L. Sturzaccess-technologyde, Multiple Equiaxed Dendrite Interaction Investigated on MASER-13, Proc. 23rd ESA Symp. Eur. Rocket Balloon Program. Relat. Res. (2017).

[35] T. Hughes, A.J. Robinson, S. McFadden, Multiple Dendrite Tip Tracking for In-Situ Directional Solidification: Experiments and Comparisons to Theory, Mater. Today Commun. 29 (2021) 102807. https://doi.org/10.1016/j.mtcomm.2021.102807.

[36] W. Kurz, M. Rappaz, R. Trivedi, Progress in modelling solidification microstructures in metals and alloys. Part II: dendrites from 2001 to 2018, Int. Mater. Rev. 66 (2021) 30–76. https://doi.org/10.1080/09506608.2020.1757894.

[37] D. Ma, Development of dendrite array growth during alternately changing solidification condition, J. Cryst. Growth. 260 (2004) 580–589. https://doi.org/10.1016/J.JCRYSGRO.2003.08.071.

[38] M. Rappaz, E. Blank, Simulation of oriented dendritic microstructures using the concept of dendritic lattice, J. Cryst. Growth. 74 (1986) 67–76. https://doi.org/10.1016/0022-0248(86)90249-6.

[39] H. Esaka, W. Kurz, R. Trivedi, Evolution of primary dendrite spacing in succinonitrile acetone alloys, Solidif. Process. Inst. Met. London. 1 (1987) 198–201.

[40] C.A. Gandin, M. Eshelman, R. Trivedi, Orientation dependence of primary dendrite spacing, Metall. Mater. Trans. A Phys. Metall. Mater. Sci. 27 (1996) 2727–2739. https://doi.org/10.1007/BF02652367.

[41] A. Wagner, B.A. Shollock, M. McLean, Grain structure development in directional solidification of nickel-base superalloys, Mater. Sci. Eng. A. 374 (2004) 270–279. https://doi.org/10.1016/j.msea.2004.03.017.

[42] L. Sturz, M. Hamacher, G. Zimmermann, In-situ observation of equiaxed dendritic growth and interaction in microgravity, proc. 6th Decennial International Conference on Solidiifcation Processing (ed. Z. Fan) (2017) 300-303

[43] N. D'souza, M.G. Ardakani, M. McLean, B.A. Shollock, Directional and single-crystal solidification of Ni-base superalloys: Part I. The role of curved isotherms on grain selection, Metall. Mater. Trans. A Phys. Metall. Mater. Sci. 31 (2000) 2877–2886. https://doi.org/10.1007/BF02830351.

[44] H. Yu, J. Li, X. Lin, L. Wang, W. Huang, Anomalous overgrowth of converging dendrites during directional solidification, J. Cryst. Growth. 402 (2014) 210–214. https://doi.org/10.1016/j.jcrysgro.2014.05.016.